Modeling and inversion of PS-wave moveout asymmetry for tilted TI media: Part I — Horizontal TTI layer

Pawan Dewangan[1] and Ilya Tsvankin[2]

ABSTRACT

One of the distinctive features of mode-converted waves is their asymmetric moveout (i.e., the PS-wave traveltime in general is different if the source and receiver are interchanged) caused by lateral heterogeneity or elastic anisotropy. If the medium is anisotropic, the PS-wave moveout asymmetry contains valuable information for parameter estimation that cannot be obtained from pure reflection modes.

Here, we generalize the so-called PP + PS = SS method, which is designed to replace reflected PS modes in velocity analysis with pure (unconverted) SS-waves, by supplementing the output SS traces with the moveout-asymmetry attributes of PS-waves. The time-asymmetry attribute Δt_{PS} is computed in the slowness domain as the difference between the paired traveltimes of the PS arrivals corresponding to ray parameters (horizontal slownesses) of equal magnitude but opposite sign. Another useful asymmetry attribute is the offset $x_{\min}$ of the PS-wave traveltime minimum on a common-midpoint (CMP) gather.

We demonstrate the effectiveness of the developed algorithm and the importance of including the asymmetry attributes of PS-waves in anisotropic velocity analysis for a horizontal transversely isotropic layer with a tilted symmetry axis (or TTI) medium. Simple analytic expressions for the moveout asymmetry of PSV-waves, derived in the weak-anisotropy approximation, are verified by anisotropic ray tracing. The attribute Δt_{PS} is proportional to the anellipticity parameter η and reaches its maximum when the symmetry axis deviates by 20°–30° from the vertical or horizontal direction.

All relevant parameters of a TTI layer can be estimated by a nonlinear inversion of the NMO velocities and zero-offset traveltimes of PP- and SS- (SVSV) waves combined with the moveout-asymmetry attributes of the PSV-wave. The inversion of pure-mode (PP and SS) moveouts alone is nonunique, while the addition of the attributes Δt_{PS} and $x_{\min}$ yields stable parameter estimates from 2D data acquired in the vertical symmetry-axis plane. If the TTI model is formed by obliquely dipping fractures, the anisotropic parameters can be inverted further for the fracture orientation and compliances.

INTRODUCTION

The complex, multidimensional nature of inverse problems in anisotropic media makes it imperative to combine different wave types in estimating medium parameters. Because the use of shear-wave sources is still relatively rare, most multicomponent data sets consist primarily of P-waves and converted PS-waves. Therefore, building anisotropic models for depth imaging is based often on supplementing P-waves with mode conversions (e.g., Tsvankin, 2001). As discussed by Thomsen (1999), Granli et al. (1999), Sheley and Schuster (2003), and others, PS-waves also proved effective in imaging beneath gas clouds, migration of steeply dipping events, and lithology discrimination.

Processing of mode conversions, however, is complicated by several factors related to the asymmetry of their raypath, reflection-point dispersal (smearing), and polarity reversals (e.g., Thomsen, 1999; Grechka and Tsvankin, 2002a; Hou and Marfurt, 2002). In particular, if the medium is either laterally heterogeneous or anisotropic without a horizontal symmetry plane, the traveltime of PS-waves does not remain the same when the source and receiver are interchanged (Pelissier et al., 1991; Thomsen, 1999; Tsvankin and Grechka, 2000). This moveout asymmetry causes serious problems in applying conventional seismic processing algorithms designed for PP reflections (normal-moveout and dip-moveout corrections, velocity analysis, stacking) to PS data.

The difficulties in processing mode conversions prompted Grechka and Tsvankin (2002a) and Grechka and Dewangan (2003) to develop the so-called PP + PS = SS method designed to construct

pseudo-SS reflections from PP and PS data without precise knowledge of the velocity model. (The constructed SS events have the correct kinematics but not the amplitudes of the SS-wave primary reflections.) Since the moveout of the computed SS-waves is symmetric, it can be combined with that of the recorded PP arrivals in anisotropic stacking-velocity tomography (Grechka et al., 2002a) or other existing velocity-analysis algorithms. This approach significantly simplifies the inversion/processing flow for multicomponent surveys, and it is effective in anisotropic velocity analysis of field data (Grechka et al., 2002b; Grechka and Dewangan, 2003).

While replacing PS-waves with pure SS reflections is advantageous from the processing viewpoint, the PP + PS = SS method does not preserve the information about the asymmetry of PS moveout. Indeed, as discussed below, the traveltime of the constructed SS arrival for each source-receiver pair is obtained from the sum of the reciprocal PS-wavetimes corresponding to the same reflection point. (The reciprocal times correspond to the PS-waves with the same absolute value but opposite signs of the projection of the slowness vector onto the reflector.) As a result, the difference between the reciprocal times that quantifies the moveout asymmetry does not contribute to the computed SS data and cannot be used in the subsequent velocity analysis. Note that the moveout asymmetry of PS reflections was used by Tsvankin and Grechka (2000, 2002) for parameter estimation in dipping TI layers with a vertical symmetry axis (VTI).

This paper demonstrates that supplementing PP and SS moveout data (the SS traveltimes are supposed to be computed from the PP + PS = SS method) with the asymmetric moveout of PS-waves can help to build an anisotropic velocity field in the depth domain without a priori information. We consider the model of a horizontal transversely isotropic layer with a tilted symmetry axis (TTI) that describes, for example, obliquely dipping, rotationally invariant (penny-shaped) fractures embedded in isotropic host rock.

Other examples of subsurface TTI formations (Figure 1) include progradational clastic or carbonate sequences (e.g., Sarg and Schuelke, 2003) and dipping shale layers near salt domes and in fold-and-thrust belts such as the Canadian Foothills (e.g., Isaac and Lawton, 1999; Vestrum et al., 1999; Grechka et al., 2001). The TTI medium is parameterized here by the velocities of P- and S-waves in the symmetry direction (V_{P0} and V_{S0}, respectively), the tilt of the symmetry axis from the vertical ν, and Thomsen's (1986) anisotropic coefficients ϵ, δ, and γ defined in the coordinate system associated with the symmetry axis (Tsvankin, 2001).

In principle, the symmetry-axis orientation and the interval parameters V_{P0}, ϵ, and δ of a TTI layer can be estimated from P-wave
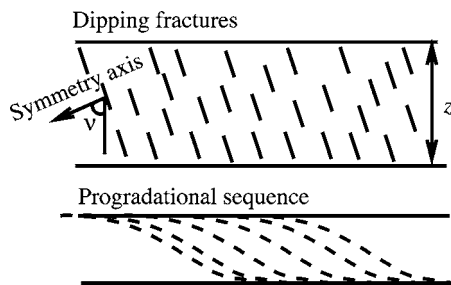

Figure 1. Horizontal TI layer with a tilted symmetry axis describes a system of dipping penny-shaped cracks embedded in an isotropic matrix as well as thin-layered progradational sequences. The results of this paper also can be applied to reflections from horizontal interfaces beneath dipping shale layers (e.g., in the Canadian Foothills).

data alone, but this inversion requires the NMO ellipses (i.e., wide-azimuth P-wave reflections) from a horizontal and a dipping interface, and both the tilt ν and reflector dip should be no less than 30°–40° (Grechka and Tsvankin, 2000). Although the addition of the NMO ellipses of pure SV-waves to those of P-waves makes it possible to invert for the TTI parameters using the reflections from a single interface, the parameter estimation is still ambiguous for a range of small tilts and reflector dips (Grechka and Tsvankin, 2000; Grechka et al., 2002a). Therefore, even wide-azimuth traveltimes of pure reflection modes (P and SV) are insufficient for constraining the parameters of horizontally layered TTI media.

The asymmetry of PS-wave moveout in a horizontal TTI layer is caused by the tilt of the symmetry axis that creates a model without a horizontal symmetry plane. The possibility of using the traveltime asymmetry of converted waves in estimating the parameters of fractured TTI media has been demonstrated on field data by Angerer et al. (2002).

In this paper, we begin by reviewing the PP + PS = SS method and then modify it to compute the asymmetry attributes of PS-waves in addition to the pure SS reflection data. Next, we study the asymmetric moveout of PS-waves in a horizontal TTI layer and develop simple linearized approximations for the time and offset asymmetry attributes. Finally, we present an inversion algorithm designed to estimate the parameters of TTI media from long-spread PP and PS reflection traveltimes and verify its accuracy and stability on noise-contaminated input data.

MODIFICATION OF THE PP + PS = SS METHOD

The PP + PS = SS method introduced by Grechka and Tsvankin (2002a) is designed for seismic surveys in which shear waves are not excited (e.g., ocean-bottom cable, or OBC) but may be recorded by multicomponent receivers. In this case, the shear wavefield is formed by mode-converted PS-waves, with the conversion often happening at the reflector. As discussed above, inversion and processing of mode conversions is hindered by their large reflection-point dispersal, polarity reversals, and moveout asymmetry.

The idea of the PP + PS = SS method is to transform the recorded PP and PS wavefields into the corresponding pure SS reflections, which are not physically generated in the survey. For anisotropic media, an important preprocessing step is Alford-type polarization analysis used to separate the converted wavefield into the fast (PS_1) and slow (PS_2) modes. The PP + PS = SS method is then applied to each split PS-wave separately with the goal of generating the fast and slow pure shear-wave reflections.

The construction of SS-waves with the correct kinematics (but not amplitudes) does not require explicit information about the velocity field, but it is necessary to correlate PP and PS arrivals and to identify the events reflected from the same interface. The original version of the PP + PS = SS method described by Grechka and Tsvankin (2002a) operates with PP and PS traveltimes picked on prestack data. As illustrated in Figure 2, matching the reflection slopes on common-receiver gathers makes it possible to find two PS rays (recorded at points $x^{(3)}$ and $x^{(4)}$) with the same reflection point as the PP reflection $x^{(1)}Rx^{(2)}$. Then the traveltime of the SS-wave is determined from

$$\tau_{SS}(x^{(3)}, x^{(4)}) = t_{PS}(x^{(1)}, x^{(3)}) + t_{PS}(x^{(2)}, x^{(4)}) - t_{PP}(x^{(1)}, x^{(2)}).$$

$$(1)$$

Application of equation 1 produces reflection SS data with the traveltimes of SS primaries but generally distorted amplitudes. The moveout of the constructed SS-waves in common-midpoint (CMP) geometry is always symmetric, as is the case for any pure reflection mode. Conventional-spread SS traveltimes are described by the NMO velocity (in two dimensions) and NMO ellipse (in three dimensions), which can be obtained using algorithms developed for PP-wave data. The NMO velocities or ellipses of the PP- and SS-waves then can be combined in velocity analysis using, for example, stacking-velocity tomography, proven to be particularly efficient for anisotropic media (Grechka et al., 2002a).

Still, for many anisotropic models including a horizontal TTI layer, pure reflection modes are not sufficient for estimating the vertical velocities and anisotropic coefficients (Grechka et al., 2002a). In such a case, an important question is whether including asymmetry attributes of the recorded PS-waves in the inversion algorithm can help in recovering the medium parameters. It is clear from equation 1 that information about the moveout asymmetry of PS arrivals is not preserved in the computed SS traveltime, which depends on only the sum of the traveltimes of the PS-waves converted at point R (Figure 2). Below, we add certain measures of the PS-wave moveout asymmetry to the traveltimes of the PP-waves and the reconstructed SS-waves.

A generalized version of the PP + PS = SS method based on equation 1 has been developed by Grechka and Dewangan (2003). Instead of operating with prestack PP and PS traveltimes, they apply a particular convolution of PP and PS traces to produce seismograms of the corresponding SS-waves. The convolution operator in the frequency domain is given by

$$W_{SS}(\omega, x^{(3)}, x^{(4)}) = \int \int W_{PS}(\omega, x^{(1)}, x^{(3)}) W_{PP}^*(\omega, x^{(1)}, x^{(2)})$$
$$\times W_{PS}(\omega, x^{(2)}, x^{(4)}) dx^{(1)} dx^{(2)}, \qquad (2)$$

where ω is the radial frequency, W_{PP} and W_{PS} are the spectra of PP and PS traces, W_{SS} is the spectrum of the constructed SS trace for the source and receiver located at points $x^{(3)}$ and $x^{(4)}$, and the * denotes complex conjugate. The integration is performed over the P-wave source and receiver coordinates $x^{(1)}$ and $x^{(2)}$ (Figure 2). The main contribution to the integral comes from the stationary point that yields the traveltime of the constructed SS-wave given by equation 1:

$$\tau_{SS}(x^{(3)}, x^{(4)}) = \min_{x^{(1)}, x^{(2)}} (t_{PS}(x^{(1)}, x^{(3)}) + t_{PS}(x^{(2)}, x^{(4)})$$
$$- t_{PP}(x^{(1)}, x^{(2)})). \qquad (3)$$

To preserve information about the moveout asymmetry of the recorded PS-wave, we suggest generating an asymmetry gather in addition to the SS data. When using the PP + PS = SS method, it is natural to define the asymmetry through the difference between the two PS traveltimes corresponding to the same reflection point (Figure 2):

$$\Delta t_{PS}(x^{(3)}, x^{(4)}) = t_{PS}(x^{(1)}, x^{(3)}) - t_{PS}(x^{(2)}, x^{(4)}). \qquad (4)$$

We modified the algorithm of Grechka and Dewangan (2003) to estimate the stationary points given by equation 3. Then the difference between the PS traveltimes (picked on the original data) corresponding to each stationary point is used to compute the time-asymmetry attribute from equation 4.

If the reflector is horizontal and the overburden is laterally homogeneous, the two reciprocal PS-waves (i.e., the waves with the raypaths $x^{(1)}Rx^{(3)}$ and $x^{(2)}Rx^{(4)}$ in Figure 2) have the same magnitude but opposite signs of the ray parameter (horizontal slowness). Hence, equation 4 defines the asymmetry of the PS moveout in the slowness domain. Analytic expressions that describe the asymmetry attribute Δt_{PS} are given in the next section.

Equation 2 can be extended to 3D multiazimuth reflection data (Grechka and Dewangan, 2003). Because sources and receivers then cover an area on the earth's surface, their coordinates **x** become two-component vectors. The integration then has to be performed over four coordinates, and the stationary point (equation 3) corresponds to a minimum in the 4D space.

ASYMMETRIC MOVEOUT OF PS-WAVES IN TTI MEDIA

Here, we use parametric representation of reflection moveout of mode-converted waves to give an analytic description of the moveout-asymmetry attributes for tilted transverse isotropy.

Parametric moveout equations

Consider a PS-wave formed by mode conversion at an interface underlying an arbitrarily anisotropic, homogeneous layer. In general, an incident P-wave in such a model excites two reflected shear modes (PS_1 and PS_2). The traveltime of either PS-wave can be represented in parametric form as (Tsvankin and Grechka, 2002)

$$t_{PS} = t_P + t_S = z(q_P - p_{1P}q_{,1P} - p_{2P}q_{,2P} + q_S - p_{1S}q_{,1S}$$
$$- p_{2S}q_{,2S}), \qquad (5)$$

where t_P and t_S are the traveltimes along the P- and S- legs, respectively, z is the depth of the reflection (conversion) point, p_1 and p_2 are
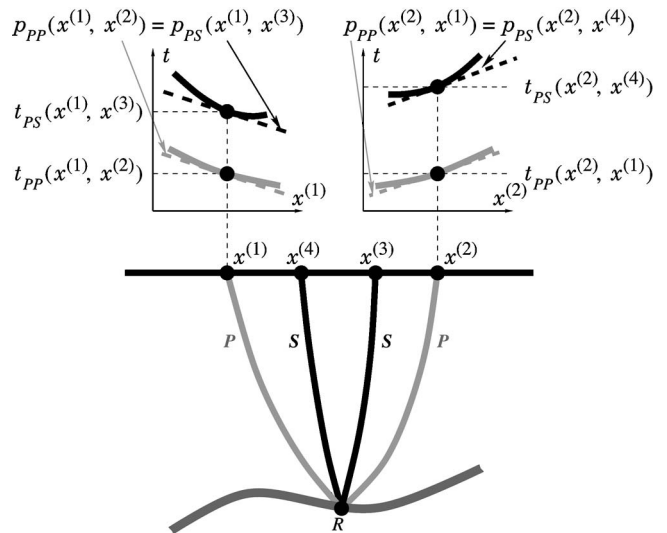

Figure 2. A 2D ray diagram of the PP + PS = SS method (after Grechka and Tsvankin, 2002a). The medium above the reflector can be arbitrarily anisotropic and heterogeneous. The reflected PP ray from $x^{(1)}$ to $x^{(2)}$ and the PS rays from $x^{(1)}$ to $x^{(3)}$ and $x^{(2)}$ to $x^{(4)}$ have the same reflection point R. The rays with the common reflection point are identified by matching the slopes on common-receiver gathers (i.e., the ray parameters) of the PP- and PS-waves.

the horizontal components of the slowness vector (the subscripts P and S indicate the wave type), $q \equiv p_3$ is the vertical slowness, and $q_{,i} \equiv \partial q / \partial p_i$ $(i = 1,2)$. Following Tsvankin and Grechka (2002), the slownesses are computed under the convention that the x_3-axis points up and both legs of the PS ray represent upgoing waves (i.e., the corresponding group-velocity vectors point toward the earth's surface).

Here, we study a horizontal layer in which the projections of the slowness vectors of the P- and S-legs onto the horizontal plane have to be identical to comply with Snell's law:

$$p_{1P} = p_1 = -p_{1S}; \quad p_{2P} = p_2 = -p_{2S}. \quad (6)$$

Equation 5 then simplifies to

$$t_{PS} = z[q_P + q_S - p_1(q_{,1P} - q_{,1S}) - p_2(q_{,2P} - q_{,2S})]. \quad (7)$$

The corresponding source-receiver vector $\mathbf{x}$ of PS-waves in an anisotropic, homogeneous layer can be also expressed through the slowness components (Tsvankin and Grechka, 2002):

$$\mathbf{x}_{PS} = \{x_1, x_2\} = z\{(q_{,1P} - q_{,1S}), (q_{,2P} - q_{,2S})\}; \quad (8)$$

where

$$x_1 = z(q_{,1P} - q_{,1S})$$

and

$$x_2 = z(q_{,2P} - q_{,2S}).$$

Equation 8 yields the source-receiver offset x_{PS} and the azimuth α of the source-receiver line with respect to the x_1-axis:

$$x_{PS} = |\mathbf{x}_{PS}| = \sqrt{x_1^2 + x_2^2}, \quad (9)$$

$$\alpha = \tan^{-1}\left(\frac{x_2}{x_1}\right). \quad (10)$$

Moveout asymmetry in the slowness domain

For laterally homogeneous models, such as a horizontal TTI layer, the moveout of converted waves becomes asymmetric only if the medium does not have a horizontal symmetry plane (e.g., Tsvankin, 2001). Conventionally, the moveout asymmetry is estimated in the offset domain by interchanging the source and receiver positions. Here, however, we define the time-asymmetry attribute in the slowness domain:

$$\Delta t_{PS} = t_{PS}(p_1, p_2) - t_{PS}(-p_1, -p_2) = \Delta t_P + \Delta t_S, \quad (11)$$

where Δt_P and Δt_S represent the contributions to Δt_{PS} from the P- and S-legs of the PS ray, respectively. Equation 11 describes the difference between the traveltimes of the PS arrivals excited by two incident P-waves that have the same magnitude ($\sqrt{p_1^2 + p_2^2}$) of the slowness vector but opposite signs of the horizontal slownesses p_1 and p_2. For a horizontal reflector beneath a laterally homogeneous medium, this definition of the time asymmetry corresponds to the two reciprocal PS-waves in the PP + PS = SS method (Figure 2).

If the moveout of PS-waves is symmetric, then changing the sign of the horizontal slowness reverses the direction of the source-re-

ceiver vector $\mathbf{x}$ (equation 8) with no change in the absolute value of offset. Hence, the measure of asymmetry for $\mathbf{x}$ can be defined in the following way:

$$\Delta \mathbf{x}_{PS} = \mathbf{x}_{PS}(p_1, p_2) + \mathbf{x}_{PS}(-p_1, -p_2). \quad (12)$$

The main advantage of treating the asymmetry in the slowness domain is that, for a laterally homogeneous medium, both Δt_{PS} and $\Delta \mathbf{x}_{PS}$ can be obtained directly from the PP + PS = SS method (see equation 4 and Figure 2).

Equations 7, 8, 11, and 12 give an exact representation of the moveout asymmetry of PS-waves for any horizontal anisotropic layer. Next, we apply this formulation to study the dependence of Δt_{PS} on the parameters of TI media with an arbitrary tilt of the symmetry axis. The offset asymmetry $\Delta \mathbf{x}_{PS}$ is discussed later, after the introduction of the offset x_{min} of the PS-wave moveout minimum in CMP geometry.

Because the contributions of the symmetry-axis orientation and anisotropic parameters to the time-asymmetry attribute Δt_{PS} are hidden in the components of the slowness vector, in Appendix A we linearize equation 11 with respect to ϵ and δ under the assumption of weak anisotropy ($|\epsilon| \ll 1$ and $|\delta| \ll 1$). The derivation is carried out for the PS mode that is polarized in the plane formed by the slowness vector and the symmetry axis. Note that although we will denote this wave PSV, its polarization vector lies in the vertical incidence plane only if that plane contains the symmetry axis.

The coordinate system is chosen in such a way that the symmetry axis is confined to the $[x_1, x_3]$ plane, which represents the only vertical symmetry plane of the model and is called here the symmetry-axis plane (Figure A-1). The sign of the time difference in equation 11 is specified by assuming that the symmetry axis is dipping in the positive x_1-direction.

Substituting equations A-5 and A-6 into equation 11, we obtain a linearized expression for the time-asymmetry attribute of the PSV-wave:

$$\Delta t_{PS} = -8\eta z V_{P0}^2 p_1[p_2^2 + (2p_1^2 + p_2^2)\cos 2\nu]\sin 2\nu, \quad (13)$$

where $\eta \equiv (\epsilon - \delta)/(1 + 2\delta) \approx \epsilon - \delta$ is the anellipticity coefficient responsible for time processing of P-wave data in VTI media (Alkhalifah and Tsvankin, 1995). In the symmetry-axis plane $[x_1, x_3]$, the slowness component p_2 vanishes, and equation 13 simplifies to

$$\Delta t_{PS}(p_2 = x_2 = 0) = -8\eta z V_{P0}^2 p_1^3 \sin 4\nu. \quad (14)$$

Using equations 13 and 14 and the results of Appendix A, the main properties of the PSV-wave time asymmetry in the slowness domain can be summarized as follows:

- The asymmetry attribute Δt_{PS} vanishes for VTI ($\nu = 0°$) and HTI ($\nu = 90°$) media because these two models have a horizontal symmetry plane. In the symmetry-axis plane, the linearized attribute Δt_{PS} (equation 14) also goes to zero for $\nu = 45°$. In this case, however, the higher-order terms in ϵ and δ (not included in equation 14) do not vanish, which makes the moveout weakly asymmetric.
- The contributions to the asymmetry attribute from the P-leg (equation A-5) and S-leg (equation A-6) of the converted wave are identical. Although this result is proved here in the weak-anisotropy approximation, numerical tests show that it remains valid for the arbitrary strength of the anisotropy.

- The asymmetry in the slowness domain depends only on the difference $\eta \approx \epsilon - \delta$ and vanishes if the anisotropy is elliptical ($\epsilon = \delta$). Because for elliptical media there is no SV-wave velocity anisotropy, the S-leg of the converted wave does not produce any moveout asymmetry. This means that the P-leg cannot cause the asymmetry either (see above).

- The magnitude of Δt_{PS} in the symmetry-axis plane (equation 14) reaches its maximum for the tilts $\nu = 22.5°$ and $\nu = 67.5°$. Therefore, Δt_{PS} is quite sensitive to the deviation of the symmetry axis from the vertical and horizontal directions.

The azimuthally varying time-asymmetry attribute computed for a typical TTI model from the exact equations 7 and 11 is displayed in Figure 3. There is a substantial variation of Δt_{PS} with the slowness component p_1 (e.g., in the x_1-direction where $p_2 = 0$), while the influence of p_2 is much weaker. Therefore, Figure 3 indicates that most of the 3D (wide-azimuth) moveout-asymmetry information can be obtained in the symmetry-axis plane $[x_1, x_3]$.

Note that the line $p_1 = 0$ in Figure 3 where $\Delta t_{PS} = 0$ does not correspond to acquisition in the $[x_2, x_3]$ plane. Because $[x_2, x_3]$ is not a symmetry plane, downgoing P-rays with $p_1 = 0$ deviate from the vertical incidence plane $[x_2, x_3]$, and the source-receiver direction of the reflected PS-wave is not parallel to the x_2-axis.

Figure 4 shows the function $\Delta t_{PS}(p_1)$ in the symmetry-axis plane in more detail. Both the PP + PS = SS method and parametric equation 11 are supposed to produce exact values of Δt_{PS}, which is confirmed by our numerical results. The magnitude of the asymmetry attribute is quite substantial; it exceeds 40% of the zero-offset time before rapidly decreasing for large values of p_1.

The accuracy of the weak-anisotropy approximation 14 in Figure 4 is quite satisfactory considering that it incorporates the contribution of the S-leg of the converted wave. Typically, the weak-anisotropy approximation is much less accurate for SV-waves than it is for P-waves because of the large magnitude of the anisotropic parameter $\sigma \equiv (V_{P0}^2/V_{S0}^2)(\epsilon - \delta)$ that controls SV-wave anisotropy (Tsvankin and Thomsen, 1994; Tsvankin, 2001). In our case, however, the an-

isotropy-related asymmetry attributes for the P- and S-legs are equal to each other (see above), and the error of the weak-anisotropy approximation is the same for both P- and S-waves.

Moveout asymmetry in the offset domain

Most existing results on the moveout asymmetry of PS-waves are obtained in the offset domain by interchanging the source and receiver positions (Thomsen, 1999; Tsvankin and Grechka, 2000, 2002). The time-asymmetry attribute in the offset domain is defined as

$$\Delta t_{PS} = t_{PS}(\mathbf{x}_{PS}) - t_{PS}(-\mathbf{x}_{PS}), \tag{15}$$

where $\mathbf{x}_{PS}$ is the offset vector of the PS-wave given by equation 8.

Azimuthally varying minimum-time offset $\mathbf{x}_{min}$

If reflection moveout is asymmetric, the minimum of the traveltime curve in a CMP gather is shifted from the CMP location. The offset x_{min} corresponding to the traveltime minimum is a convenient measure of the asymmetry that depends on the reflector orientation and medium parameters (for a numerical example, see Figure 5.7 in Tsvankin, 2001). Analytic expressions for x_{min} in a VTI layer above a dipping reflector are given by Tsvankin and Grechka (2000, 2002) and Tsvankin (2001). In a horizontal TTI layer, x_{min} carries useful information about the tilt of the symmetry axis and the anisotropic parameters.

In Appendix B, we use equations 8–10 for the offset $\mathbf{x}$ in terms of the ray parameter to obtain the following simple expression for the azimuthal variation of x_{min}:

$$x_{min}(\alpha) = x_0 \cos \alpha, \tag{16}$$

where $x_0 = x_{min}(\alpha = 0°)$ is the offset of the traveltime minimum in the symmetry-axis plane $[x_1, x_3]$ given in equation B-5:

$$x_0 = x_{min}(\alpha = 0°) = z\left[\epsilon \sin 2\nu - \frac{\eta}{2}\left(1 + \frac{V_{P0}^2}{V_{S0}^2}\right)\sin 4\nu\right]. \tag{17}$$
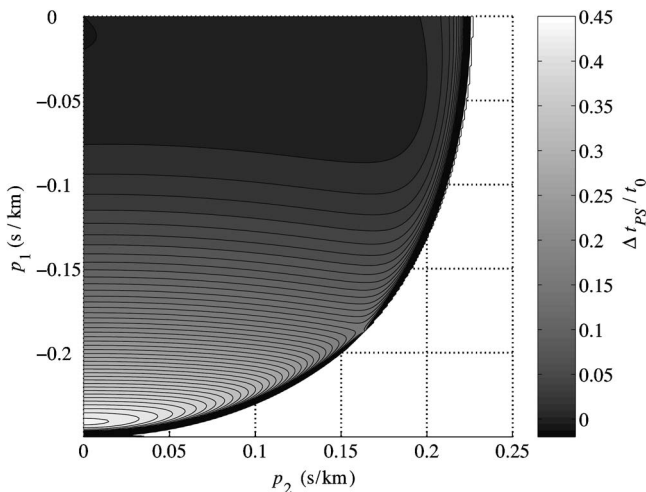

Figure 3. Exact azimuthally varying time-asymmetry attribute Δt_{PS} in the slowness domain for the PSV-wave in a horizontal TTI layer. The value Δt_{PS} is normalized by the zero-offset traveltime t_0 of the PSV-wave. The asymmetry for negative slowness p_2 is not shown because $\Delta t_{PS}(p_1, -p_2) = \Delta t_{PS}(p_1, p_2)$. The medium parameters are $V_{P0} = 4$ km/s, $V_{S0} = 2$ km/s, $\epsilon = 0.1$, $\delta = -0.1$, $\nu = 70°$, and $z = 1$ km.
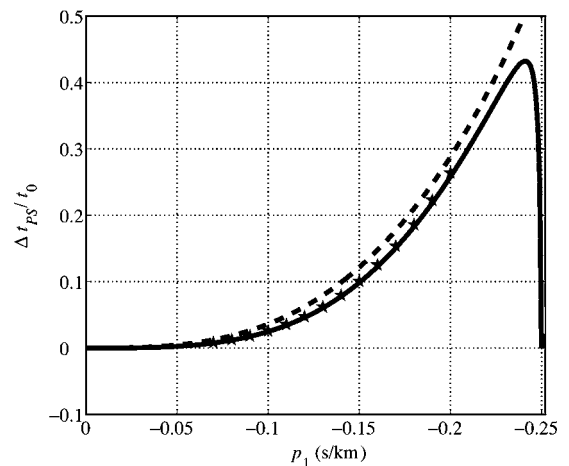

Figure 4. Asymmetry attribute Δt_{PS} from Figure 3 in the $[x_1, x_3]$ plane ($p_2 = 0$). The solid line is obtained from the exact parametric equation 11, the dashed line is the weak-anisotropy approximation 14, and the stars mark the output of the PP + PS = SS method. The maximum offset-to-depth ratio of the PP and PS data is close to two.

According to equation 16, $x_{\min}(\alpha)$ reaches its maximum in the symmetry-axis plane and vanishes in the orthogonal direction. If $x_{\min}$ is plotted as the radius vector for each azimuth α, it traces out a circle with the radius $x_0/2$ and center $(x_0, 0)$ on the x_1-axis. While equation 17 for x_0 is valid only in the weak-anisotropy limit, the azimuthal dependence of $x_{\min}$ is described by equation 16 for any strength of the anisotropy (Figure 5: similar results were obtained for much larger magnitudes of ϵ and δ). Hence, the azimuthal variation of $x_{\min}$ can help to estimate the symmetry-axis azimuth from converted-wave data, but it does not provide additional information about the anisotropic coefficients.

The offset $x_{\min}$ is not only responsible for the shape of the PS-wave moveout in CMP geometry, but it also largely controls the asymmetry measure $\Delta\mathbf{x}_{PS}$ (equation 12) defined in the slowness domain. In the symmetry-axis, plane $\Delta\mathbf{x}_{PS}$ can be written as

$$\Delta\mathbf{x}_{PS} = \mathbf{x}_{PS}(p_1, 0) + \mathbf{x}_{PS}(-p_1, 0). \qquad (18)$$

Linearizing equation 18 in the anisotropic coefficients using equation 8 yields the projection of the vector $\Delta\mathbf{x}_{PS}$ onto the x_1-axis in the form

$$(\Delta x_{PS})_{x_1} = 2x_0 + 12\eta z V_{P0}^2 p_1^2 \sin 4\nu, \qquad (19)$$

where x_0 is given by equation 17. According to equation 19, $|\Delta\mathbf{x}_{PS}|$ can be approximated by a hyperbolic function of the slowness p_1 with the value at the apex determined by $2x_0$. Indeed, when $p_1 = 0$, the PS-rays corresponding to both p_1 and $-p_1$ coincide and have the same offset x_0 (Figure 6). If the PS moveout were symmetric, the offsets for p_1 and $-p_1$ (circles and diamonds, respectively, in Figure 6) would have identical absolute values but opposite signs, and the zero-offset PS-ray would have the slowness $p_1 = 0$. Figure 6 also confirms that the linearized equation 19 is sufficiently accurate for weak and moderate anisotropy.

Therefore, an alternative way of estimating x_0 is to fit a hyperbolic function to the slowness-dependent function $(\Delta x_{PS})_{x_1}$ and find its intercept for $p_1 = 0$. It is interesting that the coefficient of the quadratic term of the hyperbola 19 is formed by the same combination of the medium parameters that governs the time-asymmetry attribute 14.

Time asymmetry in the offset domain

To give an analytic description of the attribute Δt_{PS} (equation 15) in the offset domain, we expanded the traveltime in a double Taylor series around the offset $x_{\min}$ (see Appendix C). The result is convenient to represent in terms of the azimuth α of the source-receiver line and offset x. The linearized expression C-14 for Δt_{PS} contains linear and cubic terms in the offset x and is sufficiently accurate for relatively small offsets.

This approximation can be extended to larger offsets by adapting the approach of Tsvankin and Thomsen (1994), who developed a highly accurate nonhyperbolic moveout equation for P-waves by modifying the $t^2(x^2)$ Taylor series in such a way that it became convergent at $x \to \infty$. For long-offset converted PS-waves, the incident P-wave travels almost horizontally and accounts for most of the total reflection traveltime. The contribution of the S-leg then becomes negligible, and the asymmetry attribute at infinite offset goes to zero. To ensure that Δt_{PS} vanishes for $x \to \infty$, we add a denominator $(1 + Cx^2)$ to the cubic term in equation C-14:

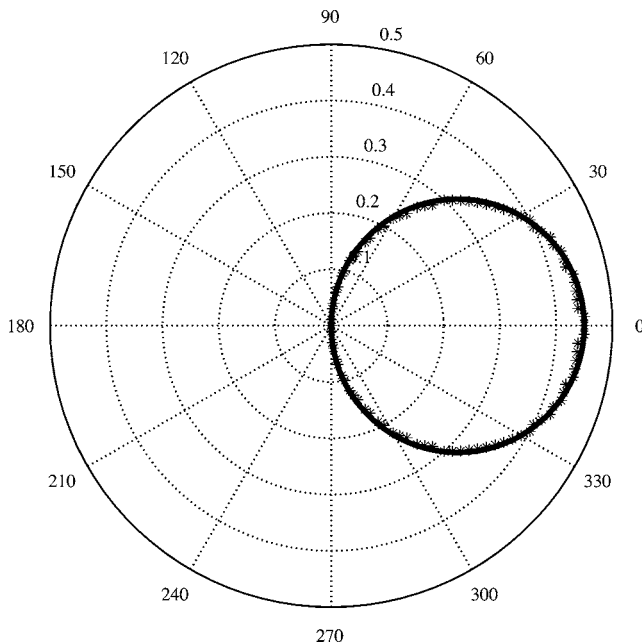$$\Delta t_{PS} = Ax + \frac{Bx^3}{1 + Cx^2}, \qquad (20)$$

Figure 5. Polar plot (in kilometers) of the offset $x_{\min}(\alpha)$ for the model from Figure 3. The stars mark values obtained from anisotropic ray tracing of PS-waves, and the solid line is computed from equation 16 with the exact value of x_0.
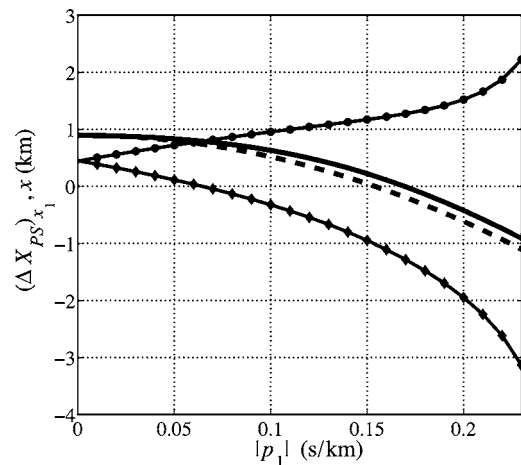

Figure 6. Slowness-domain offset-asymmetry attribute $(\Delta x_{PS})_{x_1}$ and the corresponding PS-wave offsets in the symmetry-axis plane of a TTI layer with the same parameters as those in Figure 3. The solid line marks exact values of $(\Delta x_{PS})_{x_1}$ from equation 18, and the dashed line is the weak-anisotropy approximation 19. Exact PS-wave offsets for positive slownesses p_1 are marked by circles, offsets for negative slownesses, by diamonds. The offset is considered positive if the vector $\mathbf{x}_{PS}$ points in the positive x_1-direction.

where

$$A = - \frac{2x_0 \cos \alpha}{z(V_{P0} + V_{S0})},$$

$$B = - \frac{4 \eta V_{P0}^2 \sin 2\nu \cos\alpha}{z^2(V_{P0} + V_{S0})^3}(2 \cos 2\nu \cos^2\alpha + \sin^2\alpha),$$

$$C = - \frac{B}{A}.$$

In the symmetry-axis plane ($\alpha = 0°$), the coefficients A and B in equation 20 become

$$A = - \frac{2x_0}{z(V_{P0} + V_{S0})}, \qquad (21)$$

$$B = - \frac{4 \eta V_{P0}^2 \sin 4\nu}{z^2(V_{P0} + V_{S0})^3}. \qquad (22)$$

The initial slope A of the asymmetry attribute for any azimuth α is governed by the term $(x_0 \cos \alpha)$, which represents the offset $x_{min}(\alpha)$ of the local traveltime minimum (equation 16). The higher-order coefficient B depends on the parameter $\eta \approx \epsilon - \delta$ and the tilt ν. In principle, B can be combined with A for parameter estimation. Analysis of equation 20, however, shows that the moveout asymmetry in the offset domain can be expressed through the time-asymmetry attribute Δt_{PS} in the slowness domain and the offset $x_{min}(\alpha)$.

The azimuthally varying time-asymmetry attribute in the offset domain in Figure 7 exhibits a pattern generally similar to that of Δt_{PS} in the slowness domain. The most rapid change in Δt_{PS} is observed in the $[x_1, x_3]$ plane (see also Figure 8), while in the $[x_2, x_3]$ plane the PS-wave moveout is symmetric ($\Delta t_{PS} = 0$). The absence of the moveout asymmetry for acquisition in the x_2-direction is predicted by equation 20, which yields $\Delta t_{PS} = 0$ for $\alpha = 90°$. Note that, as discussed above, PS-waves recorded in the $[x_2, x_3]$ plane have out-of-plane slowness vectors with $p_1 \neq 0$. Therefore, the lines $x_1 = 0$ in Figure 7 and $p_1 = 0$ in Figure 3 correspond to PS arrivals with different azimuthal orientations of the source-receiver vector.

The error of the weak-anisotropy approximation 20 increases with offset before flattening out at intermediate x (Figure 8) and eventually going to zero for infinitely large offsets. Overall, equation 20 gives an adequate qualitative description of the moveout asym-

metry and correctly predicts a maximum of $\Delta t_{PS}(x)$ at offsets close to the reflector depth (Figure 8). By design, equation 20 also converges toward the correct value $\Delta t_{PS} = 0$ for $x \to \infty$.

PARAMETER ESTIMATION

The goal of the inversion algorithm introduced here is to estimate the parameters of a horizontal TTI layer from PP and PS (PSV) reflection events. As emphasized by Grechka and Tsvankin (2002a) and Grechka and Dewangan (2003), effective application of the PP + PS = SS method requires acquisition of long-offset (i.e., offsets should reach at least twice the reflector depth) PP and PS data. If the offset-to-depth ratio for the recorded arrivals is less than two, the range of offsets for the constructed SS data is insufficient for obtaining a reliable estimate of the S-wave stacking velocity.

The numerical tests below prove that for a wide range of tilt angles ν of the symmetry axis, the inversion can be performed using 2D data in the symmetry-axis plane. Full-azimuth acquisition, however, can help to find the orientation of this plane, unless it is known from geological or other information. An alternative way to estimate the azimuth of the symmetry-axis plane is by analyzing the polarization direction of PS-waves at small source-receiver offsets.

Data processing

Conventional hyperbolic velocity analysis of the recorded PP data yields their stacking velocity ($V_{nmo,P}$) and zero-offset reflection traveltime (t_{P0}). Then, application of the PP + PS = SS method to the PP and PS records produces traces of pseudoshear waves that have the kinematics of the pure SS (SVSV) reflections (Grechka and Tsvankin, 2002a; Grechka and Dewangan, 2003). Therefore, processing of the constructed SS arrivals can be used to estimate the stacking velocity ($V_{nmo,S}$) and zero-offset traveltime (t_{S0}) of the SS reflections that are not excited physically in the survey. If the data have a wide range of source-receiver azimuths, it may be possible to obtain the NMO ellipses of the PP- and SS-waves (Grechka and Tsvankin, 1998; Grechka et al., 2002a).

The above methodology, described in detail by Grechka et al. (2002a), is designed to avoid complications associated with processing mode-converted waves. For some anisotropic models, the combination of PP- and SS-waves is sufficient to estimate the medium parameters without additional information. In the case of TTI media,
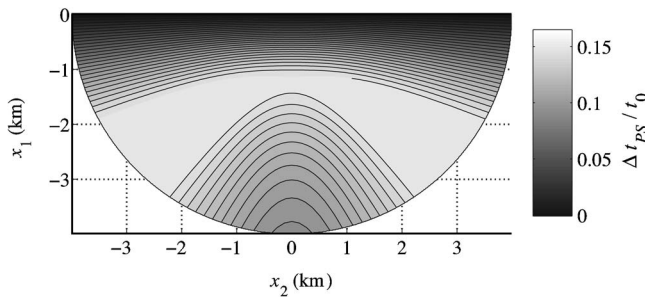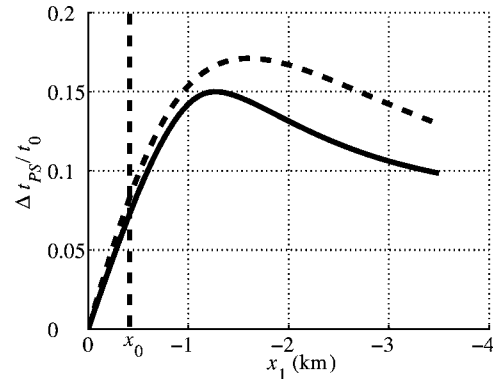

Figure 7. Exact normalized time-asymmetry attribute Δt_{PS} in the offset domain (equation 15). The data were generated by anisotropic ray tracing for the model from Figure 3. After the initial increase with offset, the asymmetry decreases for large offsets and goes to zero for $x \to \infty$.

Figure 8. Asymmetry attribute Δt_{PS} from Figure 7 in the symmetry-axis plane $x_2 = 0$. The solid line is the ray-tracing result; the dashed line is the weak-anisotropy approximation 20. Also marked is the offset $x_0 = x_{min}(\alpha = 0°)$ of the traveltime minimum.

however, the joint inversion of PP- and SS-waves is feasible only for substantial reflector dips or near-horizontal orientations of the symmetry axis (Grechka et al., 2002a).

Here, we supplement the moveouts of the PP-waves and constructed SS-waves in parameter estimation with the PS-wave asymmetry attributes obtained from the PP + PS = SS method. For laterally homogeneous media, the time asymmetry $\Delta t_{PS}(x^{(3)}, x^{(4)})$ produced by the PP + PS = SS method (equation 4) coincides with the asymmetry attribute defined in the slowness domain (equation 11). Another reason to work with the asymmetry attributes in the slowness domain is the relative simplicity of the corresponding analytic expressions.

The offset $x_{\min}(\alpha = 0)$ of the PS-wave traveltime minimum in the symmetry-axis plane $[x_1, x_3]$ can be obtained also from the PP + PS = SS method. Picking the offsets (along with the traveltimes) of the two PS-waves corresponding to the same reflection point for a range of the slownesses p_1 allows us to build the function $(\Delta x_{PS})_{x_1}(p_1)$ (equation 19). As discussed above, this function can then be approximated with a hyperbola whose apex yields the value of x_0. Alternatively, it can be shown that the offset x_0 corresponds to the PS-wave with $p_1 = 0$, whose legs coincide with the zero-offset PP and PS reflections.

Inversion algorithm

The azimuth of the symmetry-axis plane can be estimated, for example, from azimuthally varying moveout of pure (PP or SS) modes. The general equation of the NMO ellipse has the following form (Grechka and Tsvankin, 1998):

$$V_{\mathrm{nmo}}^{-2}(\alpha) = W_{11} \cos^2 \alpha + 2W_{12} \sin \alpha \cos \alpha + W_{22} \sin^2 \alpha,$$

(23)

where $W_{ij} \equiv \tau_0 \partial p_i / \partial x_j$ $(i, j = 1, 2)$, $\tau_0 \equiv t_0/2$ is the one-way zero-offset traveltime, and p_1 and p_2 are the horizontal slowness components for one-way rays from the zero-offset reflection point to the surface. All derivatives are evaluated at the CMP location. For a homogeneous horizontal layer, the matrix **W** can be represented as (Grechka et al., 1999)

$$\mathbf{W} = \frac{-q}{q_{,11}q_{,22} - q_{,12}^2} \begin{pmatrix} q_{,22} & q_{,12} \\ -q_{,12} & q_{,11} \end{pmatrix},$$

(24)

where $q \equiv q(p_1, p_2)$ is the vertical slowness and $q_{,ij} \equiv \partial^2 q / (\partial p_i \, \partial p_j)$. For pure-mode reflections, the slowness vector of the zero-offset ray for a horizontal layer is vertical, so the derivatives are computed for $p_1 = p_2 = 0$.

If the medium has a vertical symmetry plane, one of the axes of the NMO ellipse is parallel to the symmetry-plane direction (Grechka and Tsvankin, 1998). For a TTI layer with the symmetry axis confined to the $[x_1, x_3]$ plane, the terms $q_{,12}$ and W_{12} (equation 24) vanish, while W_{11} and W_{22} define the semiaxes of the NMO ellipse (equation 23). Therefore, the orientation of the NMO ellipse of the recorded PP-waves or constructed SS-waves can be used to find the azimuth of the symmetry-axis plane $[x_1, x_3]$.

Then, as described above, processing of 2D multicomponent data in the symmetry-axis plane produces the following data vector **d**:

$$\mathbf{d} \equiv \{V_{\mathrm{nmo},P}, t_{P0}, V_{\mathrm{nmo},S}, t_{S0}, \Delta t_{PS}(p_1, 0), x_0\},$$

(25)

where $x_0 \equiv x_{\min}(\alpha = 0°)$. Although $\Delta t_{PS}(p_1, 0)$ denotes multiple measurements of the asymmetry attribute for the available range of

the horizontal slownesses p_1, equation 14 indicates that the moveout asymmetry in the $[x_1, x_3]$ plane may constrain only one combination of the layer parameters.

Analytic expressions for $\Delta t_{PS}(p_1, 0)$ and $x_0 = x_{\min}(\alpha = 0°)$ needed to model these quantities in the inversion algorithm were introduced in the previous section. The NMO velocities $V_{\mathrm{nmo},P}$ and $V_{\mathrm{nmo},S}$ in the x_1-direction ($\alpha = 0°$) can be computed from equation 24 with $q_{,12} = 0$:

$$V_{\mathrm{nmo}} = \frac{1}{\sqrt{W_{11}}} = \sqrt{-\frac{q_{,11}}{q}}.$$

(26)

The model vector **m** includes the following parameters of the TTI layer:

$$\mathbf{m} \equiv \{V_{P0}, V_{S0}, \epsilon, \delta, \nu, z\}.$$

(27)

Thus, six or more [if $\Delta t_{PS}(p_1, 0)$ constrains more than one parameter] independent measurements (equation 25) are controlled by the six model parameters in equation 27. To estimate the vector **m**, we applied nonlinear inversion (the Gauss-Newton method) based on exact equations for all components of data vector 25. The misfit (objective) function minimized by the inversion algorithm is defined as

$$
\begin{aligned}
\mathcal{F} \equiv \; & w_1 \frac{(V_{\mathrm{nmo},P}^{\mathrm{calc}} - V_{\mathrm{nmo},P}^{\mathrm{meas}})^2}{(V_{\mathrm{nmo},P}^{\mathrm{meas}})^2} + w_2 \frac{(V_{\mathrm{nmo},S}^{\mathrm{calc}} - V_{\mathrm{nmo},S}^{\mathrm{meas}})^2}{(V_{\mathrm{nmo},S}^{\mathrm{meas}})^2} \\
& + w_3 \frac{(t_{P0}^{\mathrm{calc}} - t_{P0}^{\mathrm{meas}})^2}{(t_{P0}^{\mathrm{meas}})^2} + w_4 \frac{(t_{S0}^{\mathrm{calc}} - t_{S0}^{\mathrm{meas}})^2}{(t_{S0}^{\mathrm{meas}})^2} \\
& + w_5 \frac{\sum_0^p (\Delta t_{PS}^{\mathrm{calc}} - \Delta t_{PS}^{\mathrm{meas}})^2}{(\sum_0^p \Delta t_{PS}^{\mathrm{meas}})^2} + w_6 \frac{(x_0^{\mathrm{calc}} - x_0^{\mathrm{meas}})^2}{(x_0^{\mathrm{meas}})^2},
\end{aligned}
$$

(28)

where the superscripts calc and meas denote the calculated and measured quantities, respectively, and p is the maximum value of the horizontal slowness p_1. The weighting coefficients w_i were generally set to unity. We observed, however, that assigning substantially larger weights to the asymmetry attributes typically leads to a faster convergence of the algorithm.

Because the exact equations for the model parameters are nonlinear and the misfit function contains local minima, selection of the starting model may have a significant influence on the performance of the algorithm. We based the initial guesses for the vertical velocities and anisotropic coefficients on the isotropic relationships,

$$V_{P0} = V_{\mathrm{nmo},P}, V_{S0} = V_{\mathrm{nmo},S}, \epsilon = 0, \delta = 0, z = V_{\mathrm{nmo},P} t_{P0}/2.$$

(29)

Our numerical tests show that if the starting model is isotropic (equation 29) and the initial tilt ν is set to 0° or 90°, the algorithm either does not converge toward the correct solution or the convergence is extremely slow. This happens because the initial values of the partial derivatives of the objective function 28 with respect to several model parameters go to zero. The convergence can be improved significantly by keeping the initial $\epsilon = \delta = 0$ but starting with an intermediate tilt ν that is as close as possible to the actual value. For example, if the anisotropy is known to be caused by subvertical fractures, a good choice of the initial tilt is $\nu = 70°–80°$.

Numerical examples

The uniqueness and stability of the inversion was examined by applying the algorithm to noise-contaminated input data. We analyzed a representative set of TTI models with a wide range of the tilt angles ν of the symmetry axis.

Models with tilt $\nu > 60°$

TTI models with a significant tilt of the symmetry axis can be considered typical for dipping fracture sets because fracture planes seldom deviate far from the vertical (Angerer et al., 2002). For a system of vertical penny-shaped cracks in isotropic host rock, the symmetry axis is horizontal ($\nu = 90°$), and the medium becomes HTI.

The tilt $\nu = 70°$ of the symmetry axis in Figure 9 is quite favorable for the inversion based on the moveout-asymmetry attributes of PS-waves. Here and in the examples below, the data vector **d** (equation 25) was generated using the exact equations and contaminated by Gaussian noise. The inversion was carried out for 100 realizations of the input data, which allowed us to compute the standard deviations of the estimated parameters. The initial guess was based on the isotropic relationships 29, with the tilt picked randomly from the 50°–85° interval. The model vector **m** (equation 27) was estimated by minimizing the objective function specified in equation 28, as discussed in the previous section.

Figure 9 indicates that the inversion results are unbiased, and the random noise is not amplified by the parameter-estimation procedure. The standard deviations are close to 0.02 for ϵ and δ, 1% for V_{P0}, 2% for V_{S0} and z, and 1° for ν. In principle, correlated noise may cause more significant distortions of the inverted parameters. The asymmetry attributes, however, are insensitive to a nearly uniform change (near-constant shift) in the reflection traveltimes.

The best-constrained parameter combination is the difference ($\epsilon - \delta$), which controls the time-asymmetry attribute in the slowness domain (equations 13 and 14) and has a strong influence on the NMO velocity of the constructed SS-waves. Although the traveltimes of the PP- and PS-waves in the symmetry-axis plane are sufficient for estimating all relevant TTI parameters, the addition of wide-azimuth data increases the accuracy of the inversion in the presence of noise.

It should be emphasized that the parameter estimation is feasible only if the asymmetry information of the PS-wave is included in the inversion algorithm. The offset x_0 of the PS-wave moveout minimum for the model from Figure 9 reaches about one-third of the depth z, and the asymmetry attribute Δt_{PS} for the offset $x = 2z$ is about 15% of the zero-offset PS traveltime. Such a large magnitude of the time asymmetry helps to constrain the tilt of the symmetry axis and the anisotropic parameters. Without the asymmetry information, the inversion becomes unstable, even if the 2D data in the vertical symmetry plane are supplemented with the NMO ellipses of PP- and SS-waves (Grechka and Tsvankin, 2000; Grechka et al., 2002a).

Because the time asymmetry is estimated from the relatively small difference of two time measurements, it is important to evaluate the sensitivity of the inversion results to larger errors in the PS-wave asymmetry attributes. For the test in Figure 10, the standard deviations of Δt_{PS} and x_0 were increased from 2% to 4% (also, the deviations of the zero-offset times were increased to 1%). Despite the somewhat higher scatter of the inverted parameters, the standard deviations do not exceed 0.03 for ϵ and δ, 2% for V_{P0}, 3% for V_{S0} and z, and 1° for ν.

For HTI media ($\nu = 90°$) the PS-wave moveout is symmetric, and the 2D inversion in the symmetry-axis plane cannot constrain the medium parameters. However, even a small (10°) deviation of the symmetry axis from the horizontal plane creates a measurable moveout asymmetry. For the model from Figure 11, the offset x_0 is close to 20% of the depth z, and the attribute Δt_{PS} reaches about 7% of the zero-offset PS traveltime for $x = 2z$. Because the magnitude of the asymmetry attributes is smaller compared to the model with $\nu = 70°$, the error in the asymmetry attributes is expected to be higher. Figure 11 shows the inversion results when the error in Δt_{PS} and x_0 is increased from 2% to 6%. Still, the model parameters are reasonably well constrained, with the standard deviations less than 0.04 for ϵ and δ, 2% for V_{P0}, 3% for V_{S0} and z, and 1° for ν. If the symmetry axis deviates by less than 10° from either the vertical or horizontal direction, then the asymmetry attributes are too small to be estimated with reasonable accuracy and the inversion breaks down. In all the numerical tests below, the standard deviation of the noise is the same as in Figure 9.
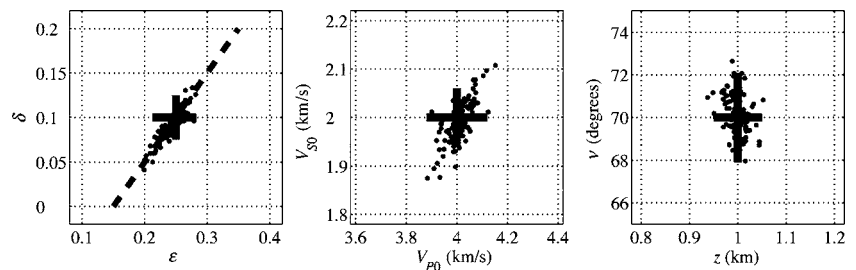

Figure 9. Inverted parameters (dots) of a horizontal TTI layer obtained from 2D PP and PS data in the symmetry-axis plane. The correct model parameters ($V_{P0} = 4$ km/s, $V_{S0} = 2$ km/s, $\epsilon = 0.25$, $\delta = 0.1$, $\nu = 70°$, $z = 1$ km) are marked by the crosses. The dashed line on the $[\epsilon, \delta]$ plot corresponds to the correct value of the difference ($\epsilon - \delta$). The input data were contaminated by Gaussian noise, with the standard deviations of 2% for the NMO velocities, 0.5% for the zero-offset traveltimes, and 2% for the PS-wave asymmetry attributes.
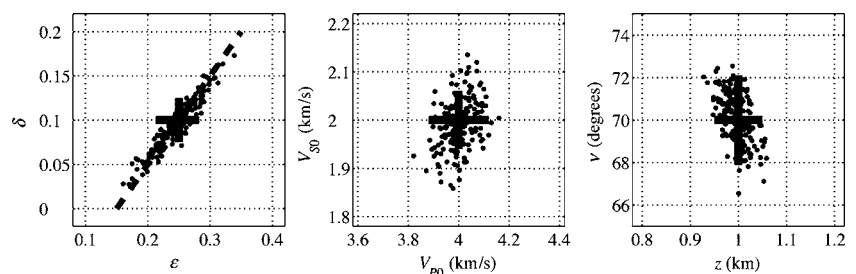

Figure 10. Same as Figure 9, but the standard deviations of the Gaussian noise are increased to 1% for the zero-offset traveltimes and 4% for the PS-wave asymmetry attributes (the standard deviations for the NMO velocities remain unchanged at 2%).

Models with intermediate tilt

The time-asymmetry attribute in the slowness domain is small not only for near-vertical and near-horizontal orientations of the symmetry axis but also for tilts ν close to 45° (equation 14). The model of a horizontal TTI layer with $35° < \nu < 55°$ can be used to describe
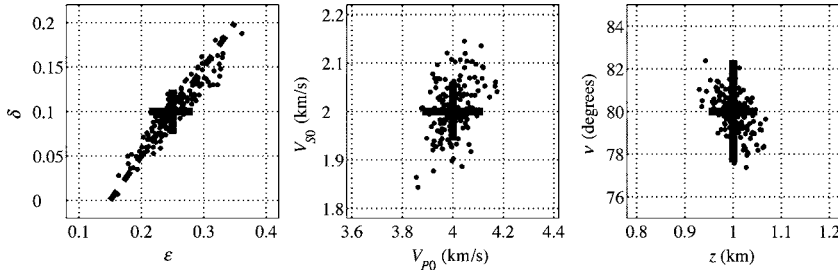

Figure 11. Inversion results for a model with the same parameters as those in Figure 9 except for the tilt $\nu = 80°$. The standard deviations of Gaussian noise here are 2% for the NMO velocities, 0.5% for the zero-offset traveltimes, and 6% for the PS-wave asymmetry attributes.
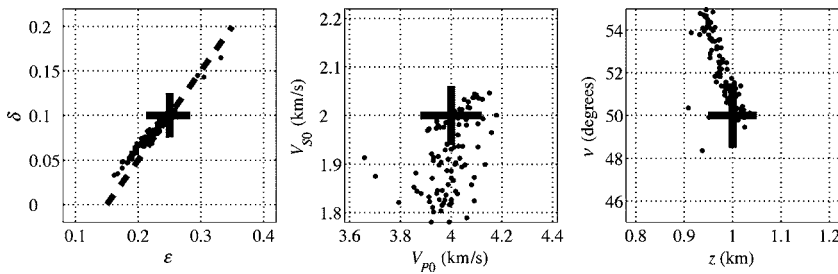

Figure 12. Inversion results for a model with the same parameters (and the same standard deviations of the noise) as those in Figure 9 except for the tilt $\nu = 50°$.
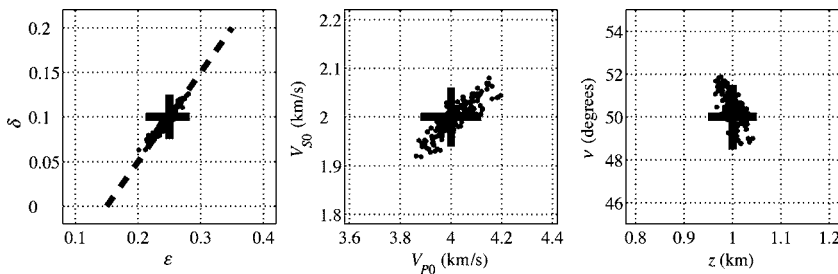

Figure 13. Same as Figure 12, but the inversion algorithm is modified to avoid local minima of the objective function.

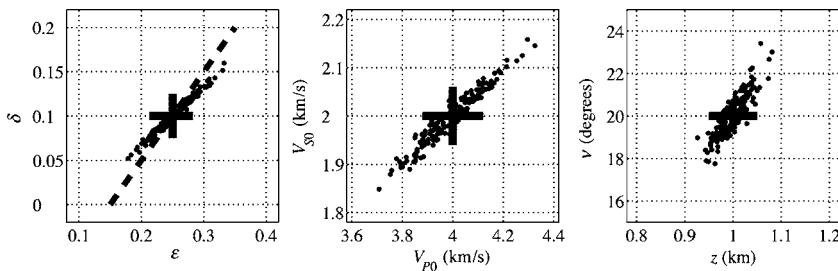Figure 14. Inversion results for a model with the same parameters as those in Figure 9 except for the tilt $\nu = 20°$.

reflections from a horizontal interface beneath dipping shale layers in fold-and-thrust belts such as the Canadian Foothills (e.g., Isaac and Lawton, 1999).

Figure 12 helps to assess the feasibility of the inversion for a tilt of 50°. Although the offset asymmetry for intermediate tilts is substantial (x_0 is about 34% of z), the inverted parameters are biased and exhibit significant scatter. Analysis of the inversion results shows that many estimated models correspond to local minima of the objective (misfit) function and do not fit the input data within the noise level.

The problem with local minima was addressed by modifying the inversion algorithm. If the search stops at a minimum where the model does not fit the data within the standard deviation of the noise (2% for the NMO velocities and the asymmetry attributes and 0.5% for the zero-offset traveltimes), then the model is perturbed to resume the search from a different point in the parameter space. Figure 13 shows that the modified algorithm produces stable inversion results for $\nu = 50°$, with the standard deviations comparable to those for $\nu = 70°$ (Figure 9).

Models with mild tilt

For completeness, here we discuss the parameter-estimation results for mild tilts ν. While such models are not plausible if the anisotropy is caused by dipping fractures, they may be adequate for effective TTI models formed by progradational sequences (e.g., Sarg and Schuelke, 2003).

The scatter in the inversion results for a tilt of 20° is slightly higher than that for large tilts, but the standard deviations are less than 0.03 for ϵ and δ, 3% for V_{P0}, V_{S0}, and z, and 2° for ν (Figure 14). As expected, the parameter estimation breaks down as the model approaches VTI, and the tilt ν becomes less than 10°. Not only do the standard deviations rapidly increase when $\nu \rightarrow 0°$, but the parameter estimates also become noticeably biased. For the model with $\nu = 5°$ in Figure 15, the bias is about 0.05 for ϵ; 0.03 for δ; and 4% for V_{P0}; V_{S0}, and z. Only the tilt is relatively well constrained by the data because of the sensitivity of the asymmetry attributes to ν.

Elliptically anisotropic models

According to our analytic results, the time asymmetry of PS-waves in the slowness domain vanishes if the medium is elliptically anisotropic (i.e., $\epsilon = \delta$). In the offset domain, however, PS moveout in elliptical media remains asymmetric and the offset $x_0 \neq 0$. Therefore, the combination of the time- and offset-asymmetry attributes used in our inversion algorithm can help to separate elliptical TTI models from VTI and HTI media, for which PS moveout is symmetric in any domain.

As illustrated by Figure 16, all parameters of an elliptically aniso-tropic layer except for the tilt are well constrained, and the standard deviations are less than 0.03 for $\epsilon = \delta$ and less than 2% for V_{P0}, V_{S0}, and z. The points on the $[\epsilon, \delta]$ plot are almost perfectly aligned along the $\epsilon = \delta$ line, which indicates that the algorithm is able to identify elliptical anisotropy. The estimates of ν, however, are more scattered (the standard deviation reaches 5°) than those for anelliptical models with the same tilt, and the average ν is biased by about 2°.

APPLICATIONS AND EXTENSIONS

Although the algorithm presented here breaks down for a horizon-tal HTI layer, parameter estimation for that model can be accom-plished using wide-azimuth PP and PS (or SS) reflection traveltimes (Tsvankin, 1997; Bakulin et al., 2000; Grechka et al., 2002a). Wide-azimuth data also help to obtain more accurate estimates of the tilt for elliptical ($\eta = 0$) TTI models. In contrast, when the symmetry axis is vertical (VTI), PP and PS reflection data do not constrain the vertical velocities ϵ and δ, even if uncommonly long offsets are used (Grechka and Tsvankin, 2002b).

Our methodology can be used for characterizing a system of dip-ping penny-shaped cracks embedded in a layer-cake isotropic medi-um (Angerer et al., 2002). Grechka and Tsvankin (2004) demon-strate that wide-azimuth seismic data can be inverted even for the pa-rameters of the more complicated model that includes penny-shaped cracks in a VTI background. Their method operates with only pure-mode reflections, but the vertical velocities are assumed to be known. It is possible that the addition of the asymmetry attributes of PS-waves to the signatures of pure PP and SS reflections can make a priori information for their model unnecessary. Note that according to the feasibility study by Grechka and Tsvankin (2003), seismic data can constrain the parameters of up to four dipping systems of penny-shaped cracks embedded in either isotropic or VTI host rock.

Tilted transverse isotropy also describes dipping shale layers in fold-and-thrust belts (such as the Canadian Foothills) and the effec-tive anisotropy of progradational sequences. While our algorithm can be applied to reflections from horizontal interfaces beneath dip-ping shales, anisotropic velocity analysis in fold-and-thrust belts may require including dipping events associated with the shale se-quence. Joint inversion of PP- and PS-waves reflected from dipping interfaces overlaid by TTI media is the subject of a companion paper (Dewangan and Tsvankin, 2006a). Another related paper (Dewan-gan and Tsvankin, 2006b) introduces a layer-stripping technique that makes it possible to extend our parameter-estimation methodology to horizontal or dipping TTI layers at depth.

CONCLUSIONS

The moveout asymmetry of mode-converted waves causes com-plications in seismic processing and can be removed by applying the PP + PS = SS method of Grechka and Tsvankin. This method makes it possible to compute the traveltimes of the primary SS re-flections (if shear waves are not excited in the survey) from PP and PS data prior to anisotropic velocity analysis. However, while the re-placement of converted waves with pure-mode SS reflections is con-venient for processing purposes, keeping information about the PS-wave moveout asymmetry may be essential for anisotropic parame-ter estimation.

Here, we presented a modification of the PP + PS = SS method designed to supplement the computed SS data with such asymmetry attributes of the converted waves as the difference Δt_{PS} between the reciprocal traveltimes in the slowness domain and the offset x_{min} of the traveltime minimum in CMP geometry. The new algorithm was applied to the inversion of multicomponent data for a horizontal TTI layer — the model used to describe the effective anisotropy caused by dipping penny-shaped cracks, dipping shale beds, or prograda-tional sequences.

Using the weak-anisotropy approximation, we obtained concise expressions for the azimuthally varying asymmetry attributes of PSV-waves in terms of the tilt ν of the symmetry axis and the anisotropic parameters ϵ and δ. For VTI ($\nu = 0°$) and HTI ($\nu = 90°$) media the PS moveout is symmetric, but the asymmetry rapidly increases as the tilt ν deviates from 0° and, espe-cially, from 90°. The asymmetry attributes also exhibit a pronounced azimuthal variation from the maximum in the symmetry-axis plane to van-ishing values in the orthogonal direction.

The asymmetry attribute Δt_{PS} in the slowness domain includes equal contributions from the P- and S-legs of the PS-wave and, in the linear ap-proximation, is proportional to the parameter $\eta \approx \epsilon - \delta$. In contrast, the offset x_{min} that quantifies the asymmetry in the offset domain depends on ϵ and δ individually and does not vanish in ellipti-cal media for which $\eta = 0$ ($\epsilon = \delta$). It is interest-ing that the azimuthal variation of x_{min} is de-scribed by a circle with the center in the symme-try-axis plane.

We combined the asymmetry attributes of PS(PSV)-waves with the NMO velocities and ze-ro-offset traveltimes of PP- and SS-waves in a nonlinear inversion algorithm (the SS travel-times are produced by the PP + PS = SS meth-od). Although it is desirable to have a wide range
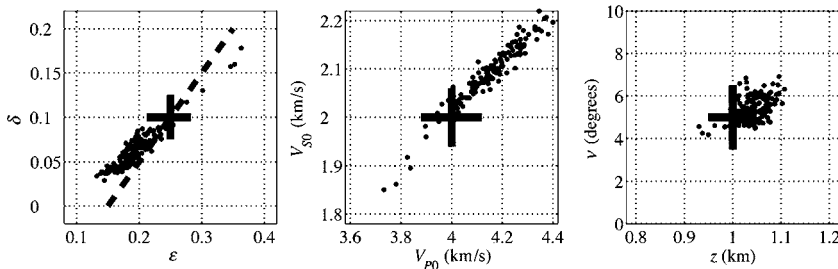

Figure 15. Inversion results for a model with the same parameters as those in Figure 9 ex-cept for the tilt $\nu = 5°$.
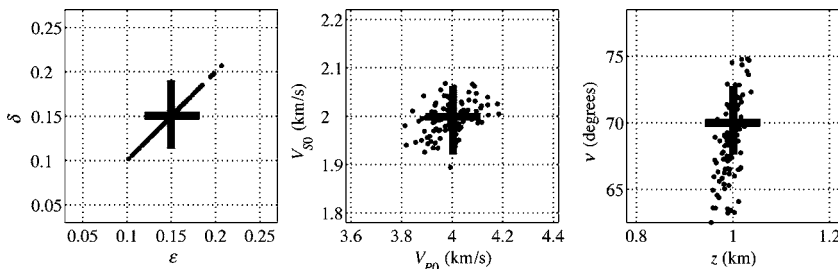

Figure 16. Inversion results for an elliptically anisotropic TTI layer with $\epsilon = \delta = 0.2$.

of source-receiver azimuths to suppress noise, the inversion can be performed using just 2D data acquired in the symmetry-axis plane. The orientation of this plane, however, must be determined beforehand from either the pure-mode NMO ellipses (i.e., from wide-azimuth data) or the PS-wave polarization at small offsets.

To assess the stability of the inversion, we ran the algorithm for multiple realizations of the input data contaminated by Gaussian noise. Without the asymmetry information, parameter estimation for a horizontal TTI layer is strongly nonunique, and a wide range of vastly different models can fit the input data. Including the PS-wave moveout asymmetry attributes removes this ambiguity and makes the 2D inversion sufficiently stable if the symmetry axis deviates by 10° or more from the vertical (VTI) and horizontal (HTI) directions.

ACKNOWLEDGMENTS

APPENDIX A

APPROXIMATE TIME-ASYMMETRY ATTRIBUTE IN THE SLOWNESS DOMAIN

For a weakly anisotropic TTI layer ($|\epsilon| \ll 1$ and $|\delta| \ll 1$), the asymmetry attribute Δt_{PS} in the slowness domain (equations 5 and 11) can be linearized in the anisotropic coefficients ϵ and δ. Without losing generality, the symmetry axis (unit vector **a**) is assumed to lie in the coordinate plane $[x_1, x_3]$ (Figure A-1):

$$\mathbf{a} \equiv [a_1, 0, a_3] = [\sin \nu, 0, \cos \nu], \quad \text{(A-1)}$$

where ν is the tilt of the symmetry axis from the vertical direction.

To obtain the vertical slowness q as a function of the horizontal slowness components p_1 and p_2 for both legs of the PS reflected ray, we use the approach suggested by Grechka and Tsvankin (2000,
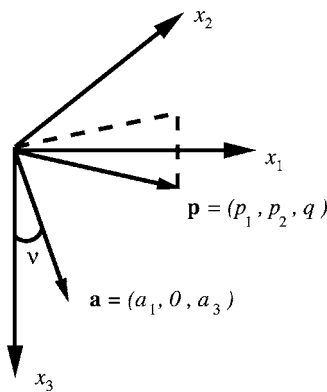

Figure A-1. The symmetry axis is defined by the unit vector **a** confined to the $[x_1, x_3]$ plane. The slowness vector **p** has an arbitrary orientation.

their Appendix B). The component q can be represented as the sum of the isotropic value $\tilde{q}$ and the anisotropy-induced correction term Δq:

$$q \equiv p_3 = \tilde{q} + \Delta q. \quad \text{(A-2)}$$

For P-waves in an isotropic medium with the velocity V_{P0}, the vertical slowness is given by

$$\tilde{q} = \sqrt{\frac{1}{V_{P0}^2} - p_1^2 - p_2^2}. \quad \text{(A-3)}$$

In the weak-anisotropy approximation Δq can be treated as the linear term in a Taylor series expansion of q in ϵ and δ for fixed horizontal slownesses p_1 and p_2:

$$\Delta q = -\frac{1}{\partial \mathcal{F}/\partial q}\left(\frac{\partial \mathcal{F}}{\partial \epsilon}\epsilon + \frac{\partial \mathcal{F}}{\partial \delta}\delta\right), \quad \text{(A-4)}$$

where $\mathcal{F}(q, p_1, p_2, V_{P0}, V_{S0}, \epsilon, \delta, \nu) = 0$ is the Christoffel equation for P- and SV-waves in TTI media.

Next, we obtain the partial derivatives $q_{,i} \equiv \partial q/\partial p_i$ ($i = 1, 2$) for the P-wave, substitute them into equations 7 and 11, and carry out further linearization using Wolfram Research's Mathematica symbolic software. The weak-anisotropy approximation for the contribution of the P-leg of the PS-wave to the asymmetry attribute has the form

$$\Delta t_P = 4z(\delta - \epsilon)p_1 V_{P0}^2 \sin 2\nu [p_2^2 + (2p_1^2 + p_2^2)\cos 2\nu]. \quad \text{(A-5)}$$

The linearized asymmetry contribution of the S-leg can be found from the P-wave equation A-5 by using the following general transformation rule (Tsvankin, 2001, p. 26):

$$V_{P0} \rightarrow V_{S0}, \epsilon \rightarrow 0, \delta \rightarrow \sigma;$$

$$\sigma \equiv \frac{V_{P0}^2}{V_{S0}^2}(\epsilon - \delta).$$

Taking into account that the asymmetry for the S-leg of a given PS-ray must be computed for the opposite sign of the horizontal slowness (so p_1 in equation A-5 has to be replaced with $-p_1$, and p_2 with $-p_2$), we find

$$\Delta t_S = -4z(\epsilon - \delta)p_1 V_{P0}^2 \sin 2\nu [p_2^2 + (2p_1^2 + p_2^2)\cos 2\nu]$$

$$= \Delta t_P. \quad \text{(A-6)}$$

APPENDIX B

AZIMUTHAL VARIATION OF THE OFFSET X_{min}

The slope dt/dx of the CMP moveout curve for any pure or converted reflection mode is determined by the difference between the projections onto the CMP line of the slowness vectors at the source and receiver locations (Tsvankin and Grechka, 2000; Tsvankin, 2001, Appendix 5B). (In this formulation, both legs of the reflected ray are treated as upgoing waves.) This general result, which is valid for any heterogeneous, anisotropic medium, can be used to find the

offset x_{min} of the PS-wave traveltime minimum where the moveout slope goes to zero. For a horizontal, laterally homogeneous layer, the horizontal slowness has the same absolute value for both legs of the reflected ray, and the slope can vanish only for a ray with the slowness vector orthogonal to the CMP line.

Suppose p_α is the projection of the slowness-vector onto the CMP line that makes the angle α with the x_1-axis and p_t is the slowness projection onto the orthogonal ($\alpha + 90°$) direction. The offset $x_{min}(\alpha)$ then corresponds to the PS ray for which $p_\alpha = 0$. Rotating the slowness vector by the angle α in the horizontal plane yields

$$p_1 = p_\alpha \cos \alpha - p_t \sin \alpha, \qquad \text{(B-1)}$$

$$p_2 = p_\alpha \sin \alpha + p_t \cos \alpha. \qquad \text{(B-2)}$$

The offset x can be parametrically represented as (equations 8 and 9)

$$x = z\sqrt{(q_{,1P} - q_{,1S})^2 + (q_{,2P} - q_{,2S})^2}. \qquad \text{(B-3)}$$

To find x_{min} from equation B-3, the derivatives $q_{,i} \equiv \partial q / \partial p_i$ ($i = 1,2$), which are derived for weakly anisotropic TTI media in Appendix A, must be evaluated for $p_\alpha = 0$.

Substituting $q_{,i}$ from Appendix A into equation B-3 and further linearizing the result in ϵ and δ produces x as a function of p_1 and p_2, which can be replaced by p_α and p_t using equations B-1 and B-2. The component p_α is then set to zero, while p_t can be found from equation 10 for the azimuth α. Linearizing equation 10 and using equations B-1 and B-2 with $p_\alpha = 0$ allows us to obtain p_t:

$$p_t = \frac{x_0 \sin \alpha}{z(V_{S0} - V_{P0})}, \qquad \text{(B-4)}$$

where $x_0 = x_{min}(\alpha = 0°)$ is the value of x_{min} in the symmetry-axis plane.

Because the slowness vectors of reflected rays propagating in the symmetry-axis plane cannot have out-of-plane components, the offset x_0 corresponds to the ray with the vertical slowness vector ($p_\alpha = p_t = p_1 = p_2 = 0$). Evaluating x from equation B-3 with $p_1 = p_2 = 0$ gives

$$x_0 = z\left[\epsilon \sin 2\nu - \frac{1}{2}(\epsilon - \delta)\left(1 + \frac{V_{P0}^2}{V_{S0}^2} \right)\sin 4\nu \right].$$
$$\text{(B-5)}$$

Finally, we substitute $p_\alpha = 0$ and p_t from equations B-4 and B-5 into equation B-3 to obtain the following expression for the azimuthally varying offset of the moveout minimum:

$$x_{min}(\alpha) = x_0 \cos \alpha. \qquad \text{(B-6)}$$

APPENDIX C

APPROXIMATE TIME-ASYMMETRY ATTRIBUTE IN THE OFFSET DOMAIN

To describe the moveout asymmetry in the offset domain defined in equation 15, we express the PS traveltime through the components x_1 and x_2 of the PS-wave offset vector $\mathbf{x}_{PS}$ (equation 8). An approximation for the asymmetry attribute in a horizontal TTI layer can be found by expanding the traveltime $t(x_1, x_2)$ in a double Taylor

series in the vicinity of the offset $(x_0, 0)$ of the moveout minimum (equation B-5):

$$t(x_1, x_2) = t(x_0, 0) + \frac{\partial t}{\partial x_1}(x_1 - x_0) + \frac{\partial t}{\partial x_2}x_2 + \frac{1}{2}\frac{\partial^2 t}{\partial x_1^2}(x_1$$

$$- x_0)^2 + \frac{1}{2}\frac{\partial^2 t}{\partial x_2^2}x_2^2 + \frac{\partial^2 t}{\partial x_1 \partial x_2}(x_1 - x_0)x_2$$

$$+ \frac{1}{3!}\frac{\partial^3 t}{\partial x_1^3}(x_1 - x_0)^3 + \frac{1}{3!}\frac{\partial^3 t}{\partial x_2^3}x_2^3$$

$$+ \frac{1}{2}\frac{\partial^3 t}{\partial x_1^2 \partial x_2}(x_1 - x_0)^2 x_2 + \frac{1}{2}\frac{\partial^3 t}{\partial x_1 \partial x_2^2}(x_1 - x_0)x_2^2$$

$$+ \ \dots \ . \qquad \text{(C-1)}$$

The traveltime derivatives in equation C-1 should be evaluated at ($x_1 = x_0$, $x_2 = 0$). Note that the first derivatives $\partial t / \partial x_1$ and $\partial t / \partial x_2$ at $(x_0, 0)$ are equal to zero.

The time-asymmetry attribute in the offset domain can be found from equation C-1 as

$$\Delta t_{PS}(x_1, x_2) = t_{PS}(x_1, x_2) - t_{PS}(-x_1, -x_2)$$

$$= -2\frac{\partial^2 t}{\partial x_1^2}x_1 x_0 - 2\frac{\partial^2 t}{\partial x_1 \partial x_2}x_2 x_0 + \frac{1}{3}\frac{\partial^3 t}{\partial x_1^3}(x_1^3$$

$$+ 3x_1 x_0^2) + x_2\left[\frac{\partial^3 t}{\partial x_1^2 \partial x_2}(x_0^2 + x_1^2) \right.$$

$$\left. + \frac{\partial^3 t}{\partial x_1 \partial x_2^2}x_1 x_2 + \frac{1}{3}\frac{\partial^3 t}{\partial x_2^3}x_2^2 \right]. \qquad \text{(C-2)}$$

Because $[x_1, x_3]$ is a plane of symmetry, $\Delta t_{PS}(x_1, x_2)$ must be an even function of x_2:

$$\Delta t_{PS}(x_1, x_2) = \Delta t_{PS}(x_1, -x_2). \qquad \text{(C-3)}$$

Therefore, equation C-2 should not contain linear and cubic terms in x_2, and

$$\frac{\partial^2 t}{\partial x_1 \partial x_2} = \frac{\partial^3 t}{\partial x_1^2 \partial x_2} = \frac{\partial^3 t}{\partial x_2^3} = 0. \qquad \text{(C-4)}$$

The second- and third-order derivatives in equation C-2 are convenient to represent in terms of the slowness components of the ray with $p_1 = p_2 = 0$ that corresponds to the offset x_0 (see Appendix B). The time slopes $\partial t / \partial x_i$ ($i = 1,2$) can be expressed through the horizontal slownesses p_1 and p_2 of the PS-wave using the results of Tsvankin (2001, Appendix 5B):

$$\frac{\partial t}{\partial x_i} = -p_i \ (i = 1,2). \qquad \text{(C-5)}$$

Differentiating $\partial t / \partial x_1$ from equation C-5 with respect to x_1 and using equation 8 yields

$$\frac{\partial^2 t}{\partial x_1^2} = \frac{\partial}{\partial x_1}\left(\frac{\partial t}{\partial x_1} \right) = \frac{-1}{\partial x_1 / \partial p_1} = \frac{-1}{z(q_{,1P,1P} - q_{,1S,1S})},$$
$$\text{(C-6)}$$

where $q_{,jP,iP} \equiv \partial^2 q_P / (\partial p_j \partial p_i)$ and $q_{,jS,iS} \equiv \partial^2 q_S / (\partial p_j \partial p_i)$.

The third-order derivatives of the traveltime t needed in equation C-2 can be obtained in a similar fashion:

$$\frac{\partial^3 t}{\partial x_1^3} = \frac{\partial}{\partial x_1}\left(\frac{-1}{\partial x_1/\partial p_1}\right)$$

$$= \frac{\partial}{\partial p_1}\left(\frac{-1}{\partial x_1/\partial p_1}\right)\left(\frac{\partial p_1}{\partial x_1}\right) + \frac{\partial}{\partial p_2}\left(\frac{-1}{\partial x_1/\partial p_1}\right)\left(\frac{\partial p_2}{\partial x_1}\right)$$

$$= \frac{q_{,1P,1P,1P} - q_{,1S,1S,1S}}{z^2(q_{,1P,1P} - q_{,1S,1S})^3}, \qquad (C\text{-}7)$$

$$\frac{\partial^3 t}{\partial x_1 \partial x_2^2} = \frac{\partial}{\partial x_1}\left(\frac{-1}{\partial x_2/\partial p_2}\right)$$

$$= \frac{\partial}{\partial p_1}\left(\frac{-1}{\partial x_2/\partial p_2}\right)\left(\frac{\partial p_1}{\partial x_1}\right)$$

$$+ \frac{\partial}{\partial p_2}\left(\frac{-1}{\partial x_2/\partial p_2}\right)\left(\frac{\partial p_2}{\partial x_1}\right)$$

$$= \frac{q_{,2P,2P,1P} - q_{,2S,2S,1S}}{z^2(q_{,2P,2P} - q_{,2S,2S})^2(q_{,1P,1P} - q_{,1S,1S})}. \qquad (C\text{-}8)$$

Here, $q_{,jP,iP,kP} \equiv \partial^3 q_P/(\partial p_j \partial p_i \partial p_k)$, $q_{,jS,iS,kS} \equiv \partial^3 q_S/(\partial p_j \partial p_i \partial p_k)$, and the derivative $(\partial p_2/\partial x_1)$ vanishes because $p_2 = 0$ on the x_1-axis.

Using the linearized derivatives of the vertical slowness q from Appendix A (equation A-2) leads to

$$\frac{\partial^2 t}{\partial x_1^2} = \frac{2}{z}\{V_{P0}[2 + \delta + \epsilon + 2\epsilon\cos 2\nu + 3(\delta - \epsilon)\cos 4\nu] \qquad (C\text{-}9)$$

$$+ V_{S0}(2 + \sigma + 3\sigma\cos 4\nu)\}^{-1}, \qquad (C\text{-}10)$$

$$\frac{\partial^3 t}{\partial x_1^3} = -\frac{12(\epsilon - \delta)V_{P0}^2 \sin 4\nu}{z^2(V_{P0} + V_{S0})^3}, \qquad (C\text{-}11)$$

$$\frac{\partial^3 t}{\partial x_1 \partial x_2^2} = -\frac{4(\epsilon - \delta)V_{P0}^2 \sin 2\nu}{z^2(V_{P0} + V_{S0})^3}. \qquad (C\text{-}12)$$

Substituting equations C-9 through C-12 into equation C-2 and further linearizing the result, we obtain the asymmetry attribute as

$$\Delta t_{PS} = -\frac{2x_1 x_0}{z(V_{P0} + V_{S0})} - \frac{4(\epsilon - \delta)V_{P0}^2 \sin 4\nu}{z^2(V_{P0} + V_{S0})^3}x_1^3$$

$$- \frac{4(\epsilon - \delta)V_{P0}^2 \sin 2\nu}{z^2(V_{P0} + V_{S0})^3}x_1 x_2^2. \qquad (C\text{-}13)$$

Finally, equation C-13 can be rewritten in terms of the offset x and the azimuth α of the source-receiver line ($x_1 = x\cos\alpha$, $x_2 = x\sin\alpha$):

$$\Delta t_{PS}(x,\alpha) = -\frac{2xx_0\cos\alpha}{z(V_{P0} + V_{S0})} - \frac{4(\epsilon - \delta)V_{P0}^2 \sin 4\nu}{z^2(V_{P0} + V_{S0})^3}x^3\cos^3\alpha$$

$$- \frac{4(\epsilon - \delta)V_{P0}^2 \sin 2\nu}{z^2(V_{P0} + V_{S0})^3}x^3\cos\alpha\sin^2\alpha$$

or

$$\Delta t_{PS}(x,\alpha) = -\frac{2xx_0\cos\alpha}{z(V_{P0} + V_{S0})} - \frac{4x^3(\epsilon - \delta)V_{P0}^2 \sin 2\nu\cos\alpha}{z^2(V_{P0} + V_{S0})^3}$$

$$\times(2\cos 2\nu\cos^2\alpha + \sin^2\alpha). \qquad (C\text{-}14)$$

REFERENCES

Alkhalifah, T., and I. Tsvankin, 1995, Velocity analysis for transversely isotropic media: Geophysics, **60**, 1550–1566.
Angerer, E., S. A. Horne, J. E. Gaiser, R. Walters, S. Bagala, and L. Vetri, 2002, Characterization of dipping fractures using PS mode-converted data: 72nd Annual International Meeting, SEG, Expanded Abstracts, 1010–1013.
Bakulin, A., V. Grechka, and I. Tsvankin, 2000, Estimation of fracture parameters from reflection seismic data — Part I: HTI model due to a single fracture set: Geophysics, **65**, 1788–1802.
Dewangan, P., and I. Tsvankin, 2006a, Modeling and inversion of PS-wave moveout asymmetry for tilted TI media: Part II – Dipping TTI layer: Geophysics, this issue.
——, 2006b, Velocity-independent layer stripping of PP and PS reflection traveltimes: Geophysics, this issue.
Granli, J. R., B. Arntsen, A. Sollid, and E. Hilde, 1999, Imaging through gas-filled sediments using marine shear-wave data: Geophysics, **64**, 668–677.
Grechka, V., and P. Dewangan, 2003, Generation and processing of pseudo shear-wave data: Theory and case study: Geophysics, **68**, 1807–1816.
Grechka, V., and I. Tsvankin, 1998, 3-D description of normal moveout in anisotropic inhomogeneous media: Geophysics, **63**, 1079–1092.
——, 2000, Inversion of azimuthally dependent NMO velocity in transversely isotropic media with a tilted axis of symmetry: Geophysics, **65**, 232–246.
——, 2002a, PP + PS = SS: Geophysics, **67**, 1961–1971.
——, 2002b, The joint nonhyperbolic moveout inversion of PP and PS data in VTI media: Geophysics, **67**, 1929–1932.
——, 2003, Feasibility of seismic characterization of multiple fracture sets: Geophysics, **68**, 1399–1407.
——, 2004, Characterization of dipping fractures in a transversely isotropic background: Geophysical Prospecting, **52**, 1–10.
Grechka, V., A. Pech, and I. Tsvankin, 2002a, Multicomponent stacking-velocity tomography for transversely isotropic media: Geophysics, **67**, 1564–1574.
Grechka, V., A. Pech, I. Tsvankin, and B. Han, 2001, Velocity analysis for tilted transversely isotropic media: A physical-modeling example: Geophysics, **66**, 904–910.
Grechka, V., I. Tsvankin, A. Bakulin, J. O. Hansen, and C. Signer, 2002b, Joint inversion of PP and PS reflection data for VTI media: A North Sea case study: Geophysics, **67**, 1382–1395.
Grechka, V., I. Tsvankin, and J. K. Cohen, 1999, Generalized Dix equation and analytic treatment of normal-moveout velocity for anisotropic media: Geophysical Prospecting, **47**, 117–148.
Hou, A., and K. J. Marfurt, 2002, Multicomponent prestack depth migration by scalar wavefield extrapolation: Geophysics, **67**, 1886–1894.
Isaac, J. H., and D. C. Lawton, 1999, Image mispositioning due to dipping TI media: A physical seismic modeling study: Geophysics, **64**, 1230–1238.
Pelissier, M. A., A. Thomas-Betts, and P. D. Vestergaard, 1991, Azimuthal variations in scattering amplitudes induced by transverse isotropy: Geophysics, **56**, 1584–1595.
Sarg, J. F., and J. S. Schuelke, 2003, Integrated seismic analysis of carbonate reservoirs: From the framework to the volume attributes: The Leading Edge, **22**, 640–645.
Sheley, D., and G. T. Schuster, 2003, Reduced-time migration of transmitted PS-waves: Geophysics, **68**, 1695–1707.
Thomsen, L., 1986, Weak elastic anisotropy: Geophysics, **51**, 1954–1966.
——, 1999, Converted-wave reflection seismology over inhomogeneous, anisotropic media: Geophysics, **64**, 678–690.
Tsvankin, I., 1997, Reflection moveout and parameter estimation for horizontal transverse isotropy: Geophysics, **62**, 614–629.

——, 2001, Seismic signatures and analysis of reflection data in anisotropic media: Elsevier Science Publ. Co., Inc.

Tsvankin, I., and V. Grechka, 2000, Dip moveout of converted waves and parameter estimation in transversely isotropic media: Geophysical Prospecting, **48**, 257–292.

——, 2002, 3D description and inversion of reflection moveout of PS-waves in anisotropic media: Geophysical Prospecting, **50**, 301–316.

Tsvankin, I., and L. Thomsen, 1994, Nonhyperbolic reflection moveout in anisotropic media: Geophysics, **59**, 1290–1304.

Vestrum, R. W., D. C. Lawton, and R. Schmid, 1999, Imaging structures below dipping TI media: Geophysics, **64**, 1239–1246.